Pseudofermion method for the exact description of fermionic environments: From single-molecule electronics to the Kondo resonance

Mauro Cirio [1,*] Neill Lambert [2,†] Pengfei Liang [1] Po-Chen Kuo [3,4] Yueh-Nan Chen [3,4]
Paul Menczel [2] Ken Funo [2] and Franco Nori [2,5,6]

[1]*Graduate School of China Academy of Engineering Physics, Haidian District, Beijing 100193, China*
[2]*Theoretical Quantum Physics Laboratory, Cluster for Pioneering Research, RIKEN, Wakoshi, Saitama 351-0198, Japan*
[3]*Department of Physics, National Cheng Kung University, 701 Tainan, Taiwan*
[4]*Center for Quantum Frontiers of Research & Technology, NCKU, 70101 Tainan, Taiwan*
[5]*Center for Quantum Computing, RIKEN, Wakoshi, Saitama 351-0198, Japan*
[6]*Physics Department, The University of Michigan, Ann Arbor, Michigan 48109-1040, USA*

(Received 30 July 2022; revised 25 May 2023; accepted 26 May 2023; published 7 July 2023)

We develop a discrete fermion approach for modeling the strong interaction of an arbitrary system interacting with continuum electronic reservoirs. The approach is based on a pseudofermion decomposition of the continuum bath correlation functions and is only limited by the accuracy of this decomposition. We show that to obtain this decomposition, one can allow for imaginary pseudofermion parameters, and strong damping in individual pseudofermions, without introducing unwanted approximations. For a noninteracting single-resonant level, we benchmark our approach against an analytical solution and an exact hierarchical-equations-of-motion approach. We also show that, for the interacting case, this simple method can capture the strongly correlated low-temperature physics of Kondo resonance, even in the difficult scaling limit, by employing matrix product state techniques.

DOI: 10.1103/PhysRevResearch.5.033011

I. INTRODUCTION

The orthodox model of strongly correlated electron transport in mesoscopic physics [1–3] considers one or more electronic reservoirs, parametrized by their spectral density, temperature, and chemical potential, coupled to an arbitrary system (typically fermionic impurities interacting with each other, or with additional, e.g., bosonic, environments). While this model can often be well described by *weak*-coupling theories, strong coupling between system and reservoirs plays an important role in molecular electronics [4], mesoscopic transport through quantum dots (artificial molecules) [5–8], and quantum thermodynamics [9–12]. While some integrable limits exist [13–15], generally speaking one must resort to numerical approaches to capture the nontrivial correlations that can build up between system and reservoirs.

Recently, several such approaches based on *discrete* fermion methods have been proposed and studied to capture this *strong*-coupling regime [16–18], partially inspired by similar techniques developed for strong coupling to bosonic environments [19–26]. The hierarchical equations of motion (HEOMs) [27–33] (which nonperturbatively account for system-bath entanglement by evolving a hierarchy of time-local equations obtained by repeatedly differentiating the system path-integral representation) have found great success for fermionic systems [34–39] and will be used as a benchmark of our results in this paper (see also related stochastic methods in Refs. [40–42]). More recently, the reaction-coordinate method [43], which nonperturbatively models the most relevant degrees of freedom of the environment, was adapted to fermionic systems and is simple and transparent, both conceptually and in terms of implementation. However, it is arguably limited as the approximations needed to treat the residual bath break down in the wide-band limit. Similarly, a recent approach [12] based on fitting the power spectrum with discrete Lorentzians shows promising results in terms of convergence, but by relying on only physical modes, it inherits limitations on the width and positivity of the Lorentzian fitting functions. Finally, other methods [44–50] build up a continuum reservoir from a finite set of discrete damped physical modes and can be combined with tensor network techniques (such as the process tensor [51–53]) for efficient construction and time evolution of system properties.

Here, we develop a "pseudofermion method" (akin to bosonic pseudomodes [20,23,24,26,54]) based on a discrete set of effective fermions which reproduce the key features of the correlation functions of the continuum bath. By employing unphysical modes with complex couplings, we model the reduced dynamics of the system by solving a Lindblad master equation in the augmented system+pseudofermion space. The use of a Lindblad form for the damping of the pseudofermions

*cirio.mauro@gmail.com
†nwlambert@gmail.com

does not, by construction, introduce any approximation. The only approximation arises from how well the total correlation function of the pseudofermions matches that of the original bath. In contrast to other methods [21,55–63], these unphysical degrees of freedom do not have a direct connection to the original physical environment allowing optimization of the modeling over an enlarged domain.

In summary, we present a conceptually simple framework to simulate nonperturbative effects in fermionic systems by using a Lindblad master equation. To show that this simplicity does not necessarily come at the expense of modeling power, we benchmark the accuracy of the method by reproducing nonequilibrium and Kondo-physics effects. We note that here the term "pseudofermion" has a different meaning than in non-Hermitian quantum mechanics [64–67].

II. FERMIONIC OPEN QUANTUM SYSTEMS

We consider a fermionic system S interacting with a fermionic Gaussian environment E described by the Hamiltonian ($\hbar = 1$)

$$H = H_S + H_E + H_I, \tag{1}$$

where H_S and

$$H_E = \sum_k \omega_k c_k^\dagger c_k \tag{2}$$

are the Hamiltonians for the system and environment (so that each environmental fermion c_k is characterized by the frequency ω_k). The interaction Hamiltonian is defined as

$$H_I = \sum_k g_k (s c_k^\dagger + c_k s^\dagger), \tag{3}$$

where g_k are the coupling strengths and s is an odd-fermion parity operator with support on the system. We assume the bath to be initially in a thermal equilibrium state

$$\rho_E^{\mathrm{eq}} \propto \exp\left[-\beta \sum_k (\omega_k - \mu) c_k^\dagger c_k\right], \tag{4}$$

with inverse temperature β and chemical potential μ.

In this context, the reduced system dynamics depends, in general, on the free-bath statistical properties encoded in correlation functions involving the fields

$$B(t) = \sum_k g_k c_k e^{-i\omega_k t} \tag{5}$$

in the interaction picture. When the free statistics is Gaussian, this dependence can be reduced down to two-point correlations, invoking Wick's theorem to write [68]

$$\rho_S(t) = \mathcal{T} \exp\left[\mathcal{F}(t, s, C^\sigma)\right] \rho_S(0), \tag{6}$$

in terms of the fermionic time ordering operator $\mathcal{T}$ (see, for example, Ref. [69], Eq. (5.84)) and the fermionic influence superoperator $\mathcal{F}(t, s, C^\sigma)$ [see Eq. (A1) in Appendix A]. This operator *exactly* describes the effects of the bath on the system through its dependence on the system-coupling operator s and the translational-invariant two-point correlation functions

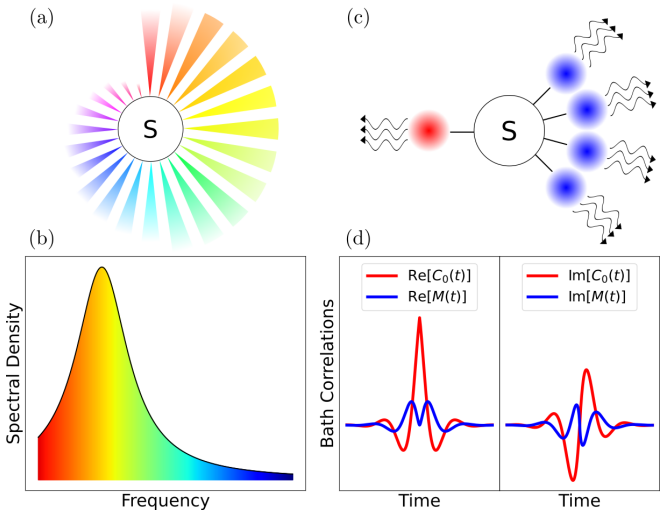

FIG. 1. Illustration of the pseudofermion model. In (a) a fermionic system S interacts with a continuum of environmental fermionic modes at different frequencies. The spectral density function in (b) describes the distribution of the system-environment coupling. As shown in (c) the dynamics of S can be equivalently computed by considering the interaction with a discrete set of pseudofermions (red and blue circles) whose dissipative properties are described by a Lindblad master equation (wiggly arrows). This equivalence holds as the pseudofermions are designed to reproduce the correlation functions of the original bath. Specifically, for the spectral density in (b), the red (blue) pseudofermions in (c) reproduce the resonant (Matsubara) contribution to the correlation function plotted in (d); see Eq. (20).

$$C^\sigma(t) = \mathrm{Tr}_E\left[B^\sigma(t) B^{\bar\sigma}(0) \rho_E^{\mathrm{eq}}\right] = \frac{1}{\pi} \int_{-\infty}^{\infty} d\omega\, J(\omega) e^{i\sigma\omega t} \left[(1-\sigma)/2 + \sigma n_E^{\mathrm{eq}}(\omega)\right]. \tag{7}$$

Here, we defined the spectral density

$$J(\omega) = \pi \sum_k g_k^2 \delta(\omega - \omega_k), \tag{8}$$

the Fermi distribution

$$n_E^{\mathrm{eq}}(\omega) = (1 + \exp[\beta(\omega - \mu)])^{-1}, \tag{9}$$

and $\sigma = \pm 1$ to denote the presence or absence of Hermitian conjugation, i.e., $B^{\sigma=1} = B^\dagger$ and $B^{\sigma=-1} = B$ (with $\bar\sigma = -\sigma$).

This analysis implies that *all memory effects* present in nonperturbative regimes can be encoded in the superoperator $\mathcal{F}(t, s, C^\sigma)$. Therefore Gaussian open systems with identical environmental correlations $C^\sigma(t)$ (and same system-coupling operators s) must have identical influence superoperators and, consequently, an equivalent reduced system dynamics through Eq. (6).

III. PSEUDOFERMION METHOD

We now proceed as schematically shown in Fig. 1(c), i.e., instead of solving the original system+continuum-environment Hamiltonian, we define a model consisting of the original system (S) in contact with a set of discrete pseudofermions (pf), themselves in contact with residual

environments (re). The key point is that our new environment (pf + re) is designed to produce the same correlation functions of the original environment, and hence produce the same system dynamics, as per Eq. (6).

To satisfactorily mimic the original correlation functions with only a finite discrete set of artificial systems, we allow certain parameters defining these pseudofermions to be unphysical. Importantly, each residual environment is an idealized quantum white noise (defined by constant spectral densities and frequency-independent equilibrium distributions), thereby allowing the dynamics in the pseudofermion space to be *exactly* described by a simple Lindblad equation [wiggly arrows in Fig. 1(c)].

Surprisingly, the use of Lindblad equations does not limit the accuracy of the result as the derivation does not rely on approximations as long as the correlation functions produced by said Lindblad equations closely match the original bath ones.

Explicitly, we consider $N_{\rm pf}$ pseudofermions $\tilde{c}_j$, $j = 1, \ldots, N_{\rm pf}$, interacting with the system as described by the Hamiltonian

$$H_{S+\rm pf} = H_S + H_{\rm pf} + \sum_{j=1}^{N_{\rm pf}} \lambda_j (s\tilde{c}_j^\dagger + \tilde{c}_j s^\dagger), \tag{10}$$

where

$$H_{\rm pf} = \sum_{j=1}^{N_{\rm pf}} \Omega_j \tilde{c}_j^\dagger \tilde{c}_j \tag{11}$$

is the free pseudofermion Hamiltonian which depends on the (formal) energies $\Omega_j \in \mathbb{C}$ and the fields

$$\tilde{B}_j^\sigma = \lambda_j \tilde{c}_j^\sigma, \tag{12}$$

in terms of the interaction strengths $\lambda_j \in \mathbb{C}$. We further assume the pseudofermions and residual environments to be initially in their equilibrium state $\rho_{\rm pf+re}^{\rm eq}$. As mentioned, the residual environment associated with each pseudofermion j is modeled as quantum white noise characterized by a formal decay rate $\Gamma_j \in \mathbb{C}$ and a formal Fermi distribution $n_j \in \mathbb{C}$. As shown in Appendix B, the free correlations in the pseudofermion and residual-environment space, i.e.,

$$C_{\rm pf}^\sigma(t) \equiv \sum_{j=1}^{N_{\rm pf}} C_{{\rm pf},j}^\sigma(t) \equiv \sum_{j=1}^{N_{\rm pf}} \lambda_j^2 {\rm Tr}_{\rm pf+re}\big[\tilde{c}_j^\sigma(t)\tilde{c}_j^{\bar{\sigma}}(0)\rho_{\rm pf+re}^{\rm eq}\big], \tag{13}$$

are defined using operators in the interaction picture, and they can be obtained by directly solving the Heisenberg equation of motion leading to

$$C_{{\rm pf},j}^\sigma(t) = \lambda_j^2[(1-\sigma)/2 + \sigma n_j]\exp[i\sigma\Omega_j t - \Gamma_j|t|]. \tag{14}$$

This result shows a main feature of the pseudofermion method: Unphysical properties (for example, the fields $\tilde{B}_j^\dagger$ *not* depending on the conjugate of the parameters λ_j) allow us to model a more general set of correlation functions [for example, $C_{{\rm pf},j}^\sigma(0) < 0$ requires λ_j to be imaginary].

Thanks to the Gaussianity hypothesis, the reduced dynamics of a system embedded in the environment made of pseudofermions and their residual environments is equivalent to the reduced dynamics of the original model with Hamiltonian H as long as

$$C^\sigma(t) = C_{\rm pf}^\sigma(t). \tag{15}$$

The practical advantage provided by this result is that, by choosing the residual environments to be idealized white noise, their effects on the system+pseudofermions space can be modeled (*without approximations*; see Ref. [68] and Appendix B) by the following Lindblad master equation:

$$\dot{\rho}_{S+\rm pf} = -i[H_{S+\rm pf}, \rho_{S+\rm pf}] + \sum_{r,j} \Gamma_j \big\{(1-n_j)D_{\tilde{c}_j}^r\big[\rho_{S+\rm pf}^r\big] + n_j D_{\tilde{c}_j^\dagger}^r\big[\rho_{S+\rm pf}^r\big]\big\}, \tag{16}$$

where $r = \pm 1$ and $j = 1 \cdots N_{\rm pf}$. Here, $\rho_{S+\rm pf}^{r=\pm}$ are the projections of the density matrix into the space with even or odd fermionic parity, and the dissipators $D_O^r[\cdot]$ are defined (see also Ref. [70]) as

$$D_O^r[\cdot] = 2rO[\cdot]O^\dagger - O^\dagger O[\cdot] - [\cdot]O^\dagger O. \tag{17}$$

This is *the main result of this paper*: When the fermionic environment of a Gaussian open quantum system has free correlations which are equivalent to (or can be approximated by) Eq. (15), the reduced system dynamics can be equivalently (approximately) computed by solving the master equation in Eq. (16).

IV. CASE STUDY: LORENTZIAN SPECTRAL DENSITY

We now provide an explicit pseudofermion model to approximate a fermionic environment initially in an equilibrium state $\rho_E^{\rm eq}$ with inverse temperature β and chemical potential μ, and where the interaction with the system is characterized by a Lorentzian spectral density

$$J_L(\omega) = \Gamma W^2/[(\omega-\mu)^2 + W^2], \tag{18}$$

where the frequency parameters W and Γ specify the width and the overall interaction strength, respectively. By inserting this expression into Eq. (7), it is possible (see Appendix B) to write the decomposition:

$$C_L^\sigma(t) = C_{\rm res}^\sigma + \sum_{k>0} M_k^\sigma(t). \tag{19}$$

Here, the "resonant" and "Matsubara" contributions are defined through

$$C_{\rm res}^\sigma(t) = \frac{\Gamma W}{2}\exp[i\sigma\mu t - W|t|],$$
$$M_k^\sigma(t) = M_k e^{-(W+x_k)|t|/2}\sum_{r=\pm} r e^{[i\sigma\mu + r(W-x_k)/2]t}, \tag{20}$$

where

$$M_k = 2i\Gamma W^2/\beta\big(x_k^2 - W^2\big), \tag{21}$$

with $x_k = (2k-1)\pi/\beta$. Our goal is to implement these contributions using a set of pseudoenvironments characterized by the free correlations in Eq. (14). To describe this correspondence, we define one *resonant* and two *Matsubara*

pseudoenvironments (for each Matsubara frequency) by identifying $j \mapsto$ res and $j \mapsto (k, r = \pm)$ in Eq. (14). This leads to the following equivalences among correlations:

$$C^{\sigma}_{\mathrm{pf,res}}(t) = C^{\sigma}_{\mathrm{res}}(t), \quad \sum_{r=\pm} C^{\sigma}_{\mathrm{pf},(k,r)}(t) = M^{\sigma}_{k}(t), \tag{22}$$

which hold (see Appendix B) when the parameters for the pseudoenvironments are defined as

$$\begin{aligned} n_{\mathrm{res}} &= 1/2, & n_{k,\pm} &= \Delta, \\ \lambda_{\mathrm{res}} &= \sqrt{\Gamma W}, & \lambda_{k,\pm} &= \sqrt{\pm M_k/\Delta}, \\ \Omega_{\mathrm{res}} &= \mu, & \Omega_{k,\pm} &= \mu \mp i(x_k - W)/2, \\ \Gamma_{\mathrm{res}} &= W, & \Gamma_{k,\pm} &= (W + x_k)/2, \end{aligned} \tag{23}$$

where $\Delta \in \mathbb{C}$ with $|\Delta| \to \infty$. We note that the limit $|\Delta| \to \infty$ might introduce numerical instabilities which can be regularized using intermediate values, such that $\Delta \gg 1$. The parameter Δ allows us to match the σ dependence between the correlations in Eqs. (20) and (14). In fact, we can note that, for $\mu = 0$, each of the Matsubara contributions in Eq. (20) does not depend on σ. On the contrary, a "particle-hole" asymmetry is present in the pseudomode correlation in Eq. (14) because of the multiplicative factor $\lambda_j^2[(1-\sigma)/2 + \sigma n_j]$. Using Eq. (23), we can see that this factor takes the σ-independent form $\pm M_k/\Delta[(1-\sigma)/2 + \sigma\Delta] \to \pm M_k$ in the limit $\Delta \to \infty$, to correctly model the "particle-hole" symmetry present in the Matsubara contribution described in Eq. (20) for $\mu = 0$.

It is important to mention that the flexibility of the method also allows for an alternative model which does not require any asymptotic limit, but uses four pseudofermions for each Matsubara contribution $M^{\sigma}_{k}(t)$. By introducing the symbols $r, \sigma' = \pm 1$, these fermionic degrees of freedom can be described by the parameters

$$\begin{aligned} n_{k,r,\sigma'} &= (1 + \sigma')/2, \\ \lambda_{k,r,\sigma'} &= \sqrt{r M_k}, \\ \Omega_{k,r,\sigma'} &= \mu - ir\sigma'(x_k - W)/2, \\ \Gamma_{k,r,\sigma'} &= (W + x_k)/2; \end{aligned} \tag{24}$$

see Appendix B.

These mappings to effective fermionic degrees of freedom are possible because of *the enlarged parameter domain of the model, which allows for complex (i.e., unphysical) values*. We can appreciate this by noting the following.

(i) M_k has a nontrivial overall complex phase requiring complex couplings $\lambda_{k,\pm}$ between the pseudomodes and the system.

(ii) M^{σ}_{k} contains terms proportional to $e^{\alpha t}$ ($\alpha \in \mathbb{R}$) which represent neither a pure physical oscillation (α is not imaginary) nor a pure physical decay (t does not appear in absolute value) ultimately requiring the pseudomodes frequencies $\Omega_{k,\pm}$ to acquire an imaginary part.

(iii) The average fermion number $n_{k,\pm}$ is, in principle, allowed to be unbounded, which implies unphysical density matrices.

The relations in Eq. (22) lead to an equivalence between the full pseudoenvironment and the original model, i.e.,

$$C^{\sigma}_{L}(t) = C^{\sigma}_{\mathrm{pf}}(t). \tag{25}$$

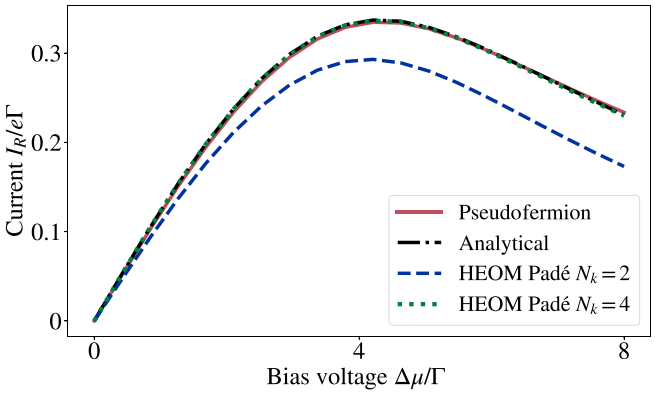

FIG. 2. Current into the right reservoir from a single impurity (coupled to two reservoirs) as a function of chemical potential difference $\Delta\mu = \mu_L - \mu_R$. For both reservoirs we choose $\epsilon = \Gamma$, $W = 2.5\Gamma$, and $\beta = 1/(0.2\Gamma)$. The truncation parameter for the HEOM results is $n_{\max} = 2$.

This shows that a fermionic environment characterized by the Lorentzian spectral density $J_L(\omega)$ can be approximated using $N_{\mathrm{pf}} = 1 + 2K_{\mathrm{pf}}$ pseudofermions. Here, K_{pf} represents a cutoff in the evaluation of the Matsubara series, i.e.,

$$\sum_{k>0} \to \sum_{k=1}^{K_{\mathrm{pf}}}, \tag{26}$$

in Eq. (19). However, when several Matsubara frequencies effectively contribute to the original correlation $C^{\sigma}_{L}(t)$ (i.e., $K_{\mathrm{pf}} \gg 1$), it might be more efficient to alternatively find a best-fit approximation of the full Matsubara series

$$M^{\sigma}(t) \equiv \sum_{k>0} M^{\sigma}_{k}(t), \tag{27}$$

following the ansatz

$$M^{\sigma} \simeq \sum_{j=1}^{K^{\mathrm{fit}}} M^{\sigma}_{j,\mathrm{fit}}(t), \tag{28}$$

where $K^{\mathrm{fit}} \in \mathbb{N}$ and

$$M^{\sigma}_{j,\mathrm{fit}}(t) \simeq M_{j,\mathrm{fit}} e^{-(W^{j}_{\mathrm{fit}} + x^{j}_{\mathrm{fit}})|t|/2} \sum_{r=\pm} r e^{[i\sigma\mu + r(W^{j}_{\mathrm{fit}} - x^{j}_{\mathrm{fit}})/2]t}, \tag{29}$$

and only then proceeding with the pseudofermion mapping, thereby optimizing the number $N^{\mathrm{fit}}_{\mathrm{pf}} = 1 + 2K^{\mathrm{fit}}$ of pseudofermions.

V. APPLICATIONS

A. Nonequilibrium single-impurity model

Our first application is a single spinless fermion coupled to two environments with Hamiltonian $H = H_S + H_E + H_I$, where

$$\begin{aligned} H_S &= \epsilon s^{\dagger} s, \\ H_E + H_I &= \sum_{\alpha,k} \omega_{\alpha,k} c^{\dagger}_{\alpha,k} c_{\alpha,k} + \sum_{\alpha} (s B^{\dagger}_{\alpha} + B_{\alpha} s^{\dagger}), \end{aligned} \tag{30}$$

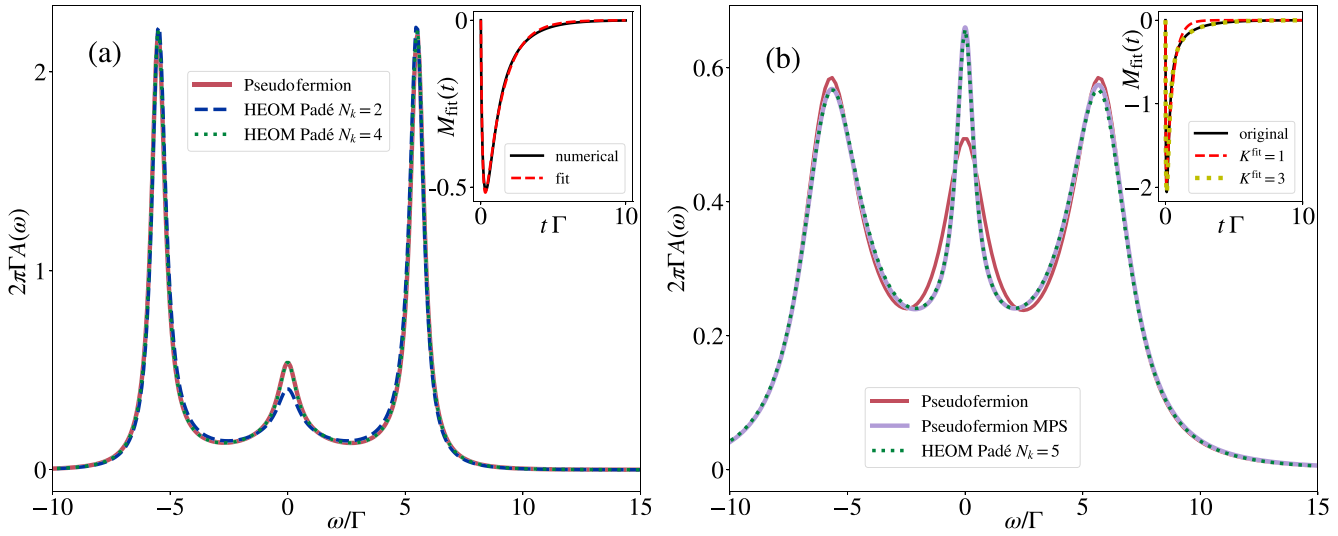

FIG. 3. Spectral density $A(\omega)$ for a single impurity containing two interacting fermions coupled to a spin-labeled reservoir. Here, $\mu = 0$, $U = 3\pi\Gamma$, $\epsilon = -U/2$, and $\beta = 1/(0.2\Gamma)$. (a) shows the results for width $W = 2.5\Gamma$, while (b) is for $W = 10\Gamma$. In (a) we see that the HEOM result with $N_k = 2$ has not converged, while all other results are (pseudofermion and HEOM, $N_k = 4$ results overlap). In (b), which uses the Matsubara series in Eq. (B49), the HEOM results converge for $N_k = 5$, while the standard pseudofermion results, relying on $K^{\rm fit} = 1$ terms in the series in Eq. (29) to fit the Matsubara contribution (shown in the inset), have not converged. To efficiently include more exponents, and hence more pseudofermions, we employ matrix product states, allowing us to include $K^{\rm fit} = 3$ terms in the Matsubara series (yellow curve in inset) and achieve convergence (solid purple curve).

with

$$B_\alpha = \sum_k g_{\alpha,k} c_{\alpha,k}, \tag{31}$$

for $\alpha \in \{L, R\}$, indexing the left and right leads. We choose both environments to be identical apart from their chemical potential, so that $J_L(\omega)$ is generalized to have an α-dependent μ_α, and we define $\Delta\mu = \mu_L - \mu_R$. We then apply the fitting procedure described in Eq. (29), so that each environment is described by $N_{\rm pf}^{\rm fit} = 1 + 2$ pseudofermions. As a benchmark we use the standard analytical result (see Ref. [14]) for the current and the HEOM method using the BOFINHEOM package [38] with a Padé decomposition of the bath exponents.

For the pseudofermions, we can evaluate the current following the logic in Refs. [36,37,71], defining the occupation of bath α as

$$N_\alpha = \sum_k c^\dagger_{\alpha,k} c_{\alpha,k} \tag{32}$$

and the current into the bath α as

$$\begin{aligned} I_\alpha(t) &= e\mathrm{Tr}[N_\alpha \dot\rho(t)] \\ &= -ie\mathrm{Tr}[\{s(t)B^\dagger_\alpha(t) + s^\dagger(t)B_\alpha(t)\}\rho(t)], \end{aligned} \tag{33}$$

in terms of the unit of charge e. In the pseudofermion formalism we equate B_α with a sum over all pseudofermions describing environment α. The equivalence of the results [72,73] for the analytical current, the HEOM method, and the pseudofermions method is demonstrated in Fig. 2.

B. Kondo resonance

To demonstrate that the pseudofermions can indeed capture nontrivial correlations between system and environment, we turn to the example of Kondo resonance [74–78]. Previously, this was used to demonstrate the power of the HEOM method in dealing with fermionic systems [35], and here we do the same for the pseudofermion method. We start with a system containing two interacting fermions labeled by their spin coupled to a spin-labeled reservoir,

$$\begin{aligned} H_S &= \epsilon(s^\dagger_\uparrow s_\uparrow + s^\dagger_\downarrow s_\downarrow) + U s^\dagger_\uparrow s_\uparrow s^\dagger_\downarrow s_\downarrow, \\ H_E + H_I &= \sum_{k,\nu} c^\dagger_{k,\nu} c_{k,\nu} + \sum_\nu s_\nu B^\dagger_\nu + B_\nu s^\dagger_\nu, \end{aligned} \tag{34}$$

where $\nu \in \{\uparrow, \downarrow\}$. The spectral density of the impurity with spin ν (an experimentally observable quantity [79,80] which can exhibit signatures of Kondo resonance) is defined as

$$A_\nu(\omega) = \frac{1}{2\pi}\int dt e^{i\omega t}\langle\{s_\nu(t), s^\dagger_\nu(0)\}\rangle. \tag{35}$$

This can be evaluated using the pseudofermion equation of motion. Figure 3 demonstrates the spectrum for a symmetric example where $U = -2\epsilon$. The pseudofermion method fits the predicted HEOM result (using a converged Padé decomposition of the bath correlation functions) remarkably well for narrow electronic bandwidths. In this case [see Fig. 3(a)] the two side peaks appear around the system energies, while the Kondo resonance appears at zero frequency, as expected.

For broader bandwidths, approaching the scaling limit, the pseudofermion model is still able to describe the main qualitative features of the Kondo peak. However, as shown in Fig. 3(b) the model does not accurately converge to the exact quantitative result with just $K^{\rm fit} = 1$. This is due to the fact

that, in order to correctly probe the low-frequency properties of the system characterizing the Kondo regime, long-time features of the correlation function become important. At very low temperatures, these features are characterized by a polynomial tail in the correlation which requires the use of more pseudofermions to capture accurately; see inset in Fig. 3(b). Since the Hilbert space of the model increases exponentially in the number of pseudofermions, standard Jordan-Wigner mappings become numerically challenging when more than a few degrees of freedom are needed, limiting the precision of the result; see the red curve in Fig. 3(b).

Fortunately, by employing matrix product state (MPS) techniques, akin to those used in Refs. [12,81], we have found that we can access this regime (see Appendix D for details on the implementation). In fact, by restricting the effective Hilbert space dimension using such a matrix product state ansatz, it is possible to improve the fitting of the slow-decaying bath correlation function and provide an accurate resolution of the zero-frequency properties of the system; see Fig. 3(b), green dotted curve.

It is interesting to note that the modeling of even broader bandwidths does not necessarily imply a further increment of the needed numerical resources. In fact, by considering the full Matsubara series $M^{\sigma}(t)$, we show in Appendix C that the terms associated with large (compared with the inverse timescales of the system) Matsubara frequencies *do not* effectively contribute to the reduced system dynamics (while for bosonic environments such terms introduce additional Markovian decay [28]). This implies that a finite truncation of the series is possible, and hence a finite number of pseudomodes can be employed even in the scaling limit.

Finally, it is important to iterate that, compared with the powerful HEOM method, the pseudofermion method produces identical results, with the advantage of a more transparent interpretation (discrete effective bath of fermions), which, as we have demonstrated, are then more intuitively amenable to MPS techniques [82,83].

VI. DISCUSSION AND SUMMARY

In this paper we presented a methodology to generate the reduced dynamics of a quantum system interacting with fermionic environments for arbitrary system-bath coupling strengths and for arbitrary bath memory times. We showed that this method allows one to accurately simulate challenging non-Markovian regimes by just solving a simple Lindblad master equation which describes the dynamics of the system coupled to ancillary "pseudofermionic" degrees of freedom. In contrast to other approaches, the presence of a Lindblad equation here does not correspond to a perturbative approximation. In fact, the method is exact as long as the correlation functions closely match the ones of the original bath. We demonstrated this balance between conceptual simplicity and numerical accuracy by reproducing the exact results of both nonequilibrium transport and Kondo resonance, benchmarked against the HEOM method. The latter is known [35] to perform as well as renormalization-group methods at finite temperatures and outperform continuous-time quantum Monte Carlo, Green's function equations of motion, and slave-boson mean-field theory. It is important to iterate that, compared with the powerful HEOM method, the pseudofermion method produces identical results, with the advantage of a more transparent interpretation (discrete effective bath fermions), which, as we have demonstrated, are then more intuitively amenable to MPS techniques [82,83].

One important feature of our approach is that the number of pseudofermion ancillas needed can be reduced by breaking certain physical constraints, resulting in an enlarged parameter space for mimicking the original environment correlation functions. To further increase the accuracy, it is possible to limit the dimension of the resulting effective Hilbert space using a matrix product state ansatz. The value of this ansatz can be seen by noting that the number of fermions needed in the model scales as $N_{\text{fermion}} = N_{\text{sys}} + (1 + 2K_{\text{fit}}) \times N_{\text{env}}$, where N_{sys} is the number of fermions needed to represent the system and N_{env} is the number of environments. In order to accurately reproduce the Kondo peak in Fig.Fig. 3, $N_{\text{sys}} = 2$, $N_{\text{env}} = 2$, and at least $K_{\text{fit}} = 3$ is needed. This corresponds to a Hilbert space of dimension 2^{16}, which can grow up to 2^{28} using the alternative decomposition in (24). Using the tensor network technique, we showed that the method can still be applied, as the matrix product state ansatz substantially reduces the number of states needed to describe the problem.

In summary, the method we have developed here can be applied to simulate the influence of non-Markovian fermionic environments strongly interacting with a quantum system with just a Lindblad master equation and an appropriate number of pseudofermion ancillas, thereby allowing challenging regimes, which traditionally require more complex numerical methods to study, to become accessible with simple open-quantum-system techniques. This method could allow one to design control or environmental-engineering protocols and to study superconducting or Majorana leads or hybrid environments (involving both fermions and bosons). Another interesting future direction is a generalization to compute bath observables and correlations to study nonequilibrium physics within the environment itself, possibly leading to the optimization of transport properties.

ACKNOWLEDGMENTS

We acknowledge Russell Deacon and Xiao Zheng for discussions and feedback. M.C. acknowledges support from NSFC (Grant No. 11935012). N.L. acknowledges partial support from JST PRESTO through Grant No. JPMJPR18GC and the Information Systems Division, RIKEN, for use of their facilities. F.N. is supported in part by Nippon Telegraph and Telephone Corporation (NTT) Research, the Japan Science and Technology Agency (JST) [via the Quantum Leap Flagship Program (Q-LEAP) and Moonshot R&D Grant No. JPMJMS2061], and the Asian Office of Aerospace Research and Development (AOARD) (via Grant No. FA2386-20-1-4069). F.N., N.L., and P.M. acknowledge the Foundational Questions Institute Fund (FQXi) via Grant No. FQXi-IAF19-06. Y.-N.C. acknowledges the support of the Ministry of Science and Technology, Taiwan (MOST Grant No. 111-2123-M-006-001). P.M. acknowledges support from the Japan Society for the Promotion of Science International Research Fellow program.

APPENDIX A: FERMIONIC OPEN QUANTUM SYSTEM

In this Appendix, we present technical details about the fermionic open quantum systems described by the original system-environment Hamiltonian $H = H_S + H_E + H_I$ used in the main text. Under the hypothesis described in the main text, the reduced system dynamics depends solely on the influence superoperator presented in Eq. (6), which can be written as

$$\mathcal{F}(t) = \sum_{\sigma=\pm} \int_0^t dt_2 \int_0^{t_2} dt_1 \mathcal{A}^\sigma(t_2)\mathcal{B}^\sigma(t_2,t_1), \tag{A1}$$

where

$$\begin{aligned} \mathcal{A}^\sigma(t)[\cdot] &= s^{\bar\sigma}(t)[\cdot] - \mathcal{P}[\cdot s^{\bar\sigma}(t)], \\ \mathcal{B}^\sigma(t_2,t_1)[\cdot] &= -C^\sigma_{21} s^\sigma(t_1)[\cdot] - \bar C^{\bar\sigma}_{21}\mathcal{P}[\cdot s^\sigma(t_1)]. \end{aligned} \tag{A2}$$

Here, we defined $s^{\sigma=-1} \equiv s$ and $s^{\sigma=1} \equiv s^\dagger$. The parity operator is defined as

$$\mathcal{P}[\cdot] = P_S[\cdot]P_S,$$

where

$$P_S = \prod_{k_S} \exp\left\{i\pi d^\dagger_{k_S} d_{k_S}\right\},$$

in terms of the fermions d_{k_S} which can populate the system. The expression of the influence superoperator explicitly shows us that the effects of the environment are fully encoded in the correlation functions $C^\sigma_{21} \equiv C^\sigma(t_2,t_1)$, where

$$\begin{aligned} C^{\sigma=1}(t_2,t_1) &= \mathrm{Tr}_E\left[B^\dagger(t_2)B(t_1)\rho_E^{\mathrm{eq}}\right] \\ &= \frac{1}{\pi}\int_{-\infty}^{\infty} d\omega J(\omega) n_E^{\mathrm{eq}}(\omega) e^{i\omega(t_2-t_1)}, \\ C^{\sigma=-1}(t_2,t_1) &= \mathrm{Tr}_E\left[B(t_2)B^\dagger(t_1)\rho_E^{\mathrm{eq}}\right] \\ &= \frac{1}{\pi}\int_{-\infty}^{\infty} d\omega J(\omega)\left[1-n_E^{\mathrm{eq}}(\omega)\right] e^{-i\omega(t_2-t_1)}, \end{aligned} \tag{A3}$$

in terms of the interaction picture operators $B(t) = \sum_k g_k c_k e^{-i\omega_k t}$, the spectral density $J(\omega) = \pi\sum_k g_k^2\delta(\omega-\omega_k)$, and the Fermi distribution $n_E^{\mathrm{eq}}(\omega) = (1+\exp\{\beta(\omega-\mu)\})^{-1}$ (in which μ represents the chemical potential). These definitions are the explicit version of the ones in Eq. (7) upon noticing that the invariance of ρ_E^{eq} under the free evolution of the bath implies time-translational invariance for the correlations.

APPENDIX B: PSEUDOFERMION MODEL

In this Appendix we present details about the pseudofermion model presented in the main text. The model is an approximation scheme which operates in an augmented Hilbert space involving ancillary pseudofermions. The prefix *pseudo* highlights the absence of physicality constraints other than the requirement to generate the correct reduced system dynamics.

Explicitly, we consider N_{pf} pseudofermions $\tilde c_j$, $j = 1,\ldots,N_{\mathrm{pf}}$, each interacting with its own residual bath of fermions $\tilde c_{jk}$ defining a formal open quantum system with Hamiltonian

$$H^{\mathrm{tot}}_{S+\mathrm{pf}} = H_{S+\mathrm{pf}} + H_{\mathrm{RE}}. \tag{B1}$$

Here,

$$H_{S+\mathrm{pf}} = H_S + H_{\mathrm{pf}} + H^I_{S+\mathrm{pf}} \tag{B2}$$

is the free Hamiltonian in the augmented system+pseudofermions space, where

$$H_{\mathrm{pf}} = \sum_{j=1}^{N_{\mathrm{pf}}} \Omega_j \tilde c^\dagger_j \tilde c_j \tag{B3}$$

is the free pseudofermion Hamiltonian which depends on the (formal) energies $\Omega_j \in \mathbb{C}$ and where

$$\begin{aligned} H^I_{S+\mathrm{pf}} &= \sum_{j=1}^{N_{\mathrm{pf}}} \lambda_j (s\tilde c^\dagger_j + \tilde c_j s^\dagger) \equiv \sum_{j=1}^{N_{\mathrm{pf}}} (s\tilde B^\dagger_j + \tilde B_j s^\dagger), \\ H_{\mathrm{RE}} &= \sum_{j,k}^{N_{\mathrm{pf}}} [\Omega_{jk}\tilde c^\dagger_{jk}\tilde c_{jk} + \lambda_{jk}(\tilde c^\dagger_j \tilde c_{jk} + \tilde c^\dagger_{jk}\tilde c_j)] \end{aligned} \tag{B4}$$

are the system + pseudofermions and pseudofermions + residual-environment interaction Hamiltonians written in terms of the fields

$$\tilde B^\sigma_j(t) = \lambda_j \tilde c^\sigma_j(t), \tag{B5}$$

the energies $\Omega_{jk} \in \mathbb{R}$, and the interaction strengths $\lambda_j \in \mathbb{C}$, $\lambda_{jk} \in \mathbb{R}$.

We further assume each auxiliary environment to act as an idealized white noise defined by constant spectral densities

$$J_j(\omega) = \pi\sum_k \lambda^2_{jk}\delta(\omega-\Omega_{jk}) = \Gamma_j, \tag{B6}$$

written in terms of the rates $\Gamma_j \in \mathbb{C}$, and by constant (frequency independent) equilibrium distributions

$$n^{\mathrm{eq}}_{jk} = n_j, \tag{B7}$$

where $n_j \in \mathbb{C}$; see Eq. (B26). Following the ideas introduced in Ref. [25] for the bosonic case, while some of the parameters in this formal model are allowed to take complex values, the dynamics is still defined using the same Schrödinger equation *as if all parameters were physical*, i.e., without introducing any extra complex conjugation, hence taking the name pseudo-Schrödinger equation [85]. This allows us to use an *unphysical* model to simulate a wider range of free correlation functions without adding extra complexity. To conclude its characterization, we assume the pseudoenvironment to be initially in its equilibrium state $\rho_{\mathrm{pf+re}}$; see Eq. (B21).

1. A pseudoenvironment

The pseudoenvironment described by the Hamiltonian

$$H_{S+\mathrm{pf}} = H_S + H_{\mathrm{pf}} + H^I_{S+\mathrm{pf}} \tag{B8}$$

is supposed to be, initially, in the following equilibrium state:

$$\rho_{\mathrm{pf+re}} = Z^{-1}_{\mathrm{pf+re}} \exp \sum_{j=1}^{N_{\mathrm{pf}}} \left[\beta_j\Omega_j\tilde c^\dagger_j\tilde c_j + \sum_k \beta_{jk}\Omega_{jk}\tilde c^\dagger_{jk}\tilde c_{jk}\right], \tag{B9}$$

in which $Z_{\text{pf+re}}$ ensures that the trace is 1 and where each $\beta_j, \beta_{jk} \in \mathbb{R}$ can be found by imposing

$$\text{Tr}_{\text{pf}}[\tilde{c}_j^\dagger \tilde{c}_j \rho_{\text{pf}}] = n_j,$$

on top of the already stated white-noise assumption

$$n_j^{\text{eq}} = \text{Tr}_{\text{pf}}[\tilde{c}_{jk}^\dagger \tilde{c}_{jk} \rho_{\text{pf}}] = n_j.$$

This leads to

$$\beta_j \Omega_j = \beta_{jk} \Omega_{jk} = \log_{10}(1/n_j - 1), \tag{B10}$$

which concludes the characterization of this "pseudoenvironment." We note that the condition in Eq. (B10) allows us to write the exponent defining $\rho_{\text{pf+re}}$ as a weighted sum over the total number of fermions in the different pseudoenvironments, which is a constant of motion under the free evolution induced by $H_{\text{pf+re}} = H_{\text{pf}} + H^I_{S+\text{pf}} + H_{\text{re}}$ (as it only contains interaction terms which are written in a "rotating wave" style, i.e., they preserve the total number of bare excitations).

2. Computing the correlation functions through the Heisenberg equation of motion

The most direct way to compute the correlations in Eq. (13) is through the Heisenberg equation of motion. For clarity, in this section we will be omitting the label j used throughout the main text to describe independent pseudoenvironments. In fact, we will be focusing on a single pseudofermion $\tilde{c}$ and its residual environment made of fermions $\tilde{c}_k$. With this notation, the free Hamiltonian of the environment, i.e., the part of the Hamiltonian in Eq. (B8) which has no support on the system, reads

$$\begin{aligned} H_{\text{pf+re}} &= H_{\text{pf}} + H^I_{\text{S+pf}} + H_{\text{RE}} \\ &= \Omega \tilde{c}^\dagger \tilde{c} + \sum_k \lambda_k (\tilde{c}^\dagger \tilde{c}_k + \tilde{c}_k^\dagger \tilde{c}) + \sum_k \Omega_k \tilde{c}_k^\dagger \tilde{c}_k, \end{aligned} \tag{B11}$$

with $J(\omega) = \pi \sum_k \lambda_k^2 \delta(\omega - \Omega_k) = \Gamma$. Using $\{\tilde{c}, \tilde{c}^\dagger\} = 1$, we obtain

$$\begin{aligned} \dot{\tilde{c}} &= i\big[H_E^{\text{pf}}, d\big] = -i\Omega\tilde{c} - i\sum_k \lambda_k \tilde{c}_k, \\ \dot{c}_k &= i\big[H_E^{\text{pf}}, \tilde{c}_k\big] = -i\Omega_k \tilde{c}_k - i\lambda_k \tilde{c}, \end{aligned} \tag{B12}$$

which, in Laplace space, becomes

$$\begin{aligned} s\tilde{c} &= \tilde{c}(0) - i\Omega\tilde{c} - i\sum_k \lambda_k \tilde{c}_k, \\ s\tilde{c}_k &= \tilde{c}_k(0) - i\Omega_k \tilde{c}_k - i\lambda_k \tilde{c}. \end{aligned} \tag{B13}$$

Substituting

$$\tilde{c}_k = (\tilde{c}_k(0) - i\lambda_k \tilde{c})/(s + i\Omega_k)$$

into the first equation, we get

$$\left[s + i\Omega + \sum_k \frac{\lambda_k^2}{s + i\Omega_k} \right] \tilde{c} = \tilde{c}(0) - \sum_k \frac{i\lambda_k}{s + i\Omega_k} \tilde{c}_k(0). \tag{B14}$$

This equation can be made more explicit by computing

$$\begin{aligned} \sum_k \frac{\lambda_k^2}{s + i\Omega_k} &= \frac{1}{\pi} \int_{-\infty}^{\infty} d\omega \frac{J(\omega)}{s + i\omega} \\ &= \frac{\Gamma}{\pi} \int_{-\infty}^{\infty} \frac{d\omega}{s + i\omega} \\ &= -i\frac{\Gamma}{\pi} \int_{-\infty}^{\infty} \frac{d\omega}{\omega - is}. \end{aligned} \tag{B15}$$

To proceed, we consider

$$\begin{aligned} \int_{-W}^{W} d\omega \frac{1}{\omega - is} &= \log_{10}\left(\frac{|W - is|}{|-W - is|} \right) \\ &\quad + \arg(W - is) - \arg(-W - is), \end{aligned} \tag{B16}$$

so that

$$\begin{aligned} \lim_{W\to\infty} \int_{-W}^{W} \frac{d\omega}{\omega - is} &= i\pi \qquad \text{for} \quad \text{Re}(s) > 0 \\ &= -i\pi \qquad \text{for} \quad \text{Re}(s) < 0. \end{aligned} \tag{B17}$$

Which of these two alternatives should we use in Eq. (B14)? The choice depends on whether we are interested in evaluating the dynamics of $\tilde{c}(t)$ for $t > 0$ or $t < 0$. For $t > 0$, we should choose the condition $\text{Re}(s) > 0$ as it is always compatible with the integration path needed to define the inverse Laplace transform. For $t < 0$, the opposite choice must be made. This means that

$$(s + i\Omega \pm \Gamma)\tilde{c} = \tilde{c}(0) - i\sum_k \frac{\lambda_k}{s + i\Omega_k} \tilde{c}_k(0), \tag{B18}$$

where the $\pm$ depends on whether $t > 0$ or $t < 0$. A similar result holds for the conjugate

$$(s - i\Omega \pm \Gamma)\tilde{c} = \tilde{c}^\dagger(0) + i\sum_k \frac{\lambda_k}{s - i\Omega_k} \tilde{c}_k^\dagger(0). \tag{B19}$$

Note that even if some of the original parameters Ω and Γ might be complex, no complex conjugation is introduced on them, as a pseudo-Schrödinger equation is used to generate the dynamics.

Our goal is now to use Eqs. (B18) and (B19) to compute the correlations in Eq. (13), which read

$$C^\sigma(t_2, t_1) = \lambda^2 \text{Tr}[\tilde{c}^\sigma(t_2) \tilde{c}^{\bar{\sigma}}(t_1) \rho_{\text{pf+re}}], \tag{B20}$$

where $\tilde{c}(t) = \exp\{iH_E^{\text{pf}} t\} \tilde{c} \exp\{-iH_E^{\text{pf}} t\}$ and where

$$\rho_{\text{pf+re}} = \exp\{-\beta\Omega \tilde{c}^\dagger \tilde{c}\} \prod_k \exp\{-\beta_k \Omega_k \tilde{c}_k^\dagger \tilde{c}_k\} / Z_{\text{pf+re}}, \tag{B21}$$

where

$$Z_{\text{pf+re}} = (e^{-\beta\Omega} + 1) \prod_k (e^{-\beta_k \Omega_k} + 1),$$

together with the constraints in Eq. (B10), i.e.,

$$\beta\Omega = \beta_k \Omega_k = \log_{10}(1/n - 1). \tag{B22}$$

Note that these constraints are essential to ensure invariance under time translation of the correlation. In fact, using them, the equilibrium state takes the form

$$\rho_{\text{pf+re}} \propto \exp\{-\beta\Omega N_E\},$$

as a function of the total number of fermions in the structured environment

$$N_{\mathrm{pf+re}} = \tilde{c}^\dagger \tilde{c} + \sum_k \tilde{c}_k^\dagger \tilde{c}_k.$$

This number is conserved by the free dynamics, i.e., $[H_{\mathrm{pf}}, N_{\mathrm{pf}}] = 0$, which implies that

$$\begin{aligned} C^\sigma(t_2, t_1) &= C^\sigma(t_2 - t_1, 0) \\ &\equiv C^\sigma(t_2 - t_1) \\ &= \lambda^2 \mathrm{Tr}[\tilde{c}^\sigma(t)\tilde{c}^{\bar{\sigma}}(0)\rho_{\mathrm{pf+re}}], \end{aligned} \tag{B23}$$

where $t = t_2 - t_1$. Therefore, using Eqs. (B18) and (B19), we can immediately compute

$$\begin{aligned} C^\sigma(t) = {} & \lambda^2 \theta(t) \mathcal{L}_t^{-1} \frac{\mathrm{Tr}[\tilde{c}^\sigma(0)\tilde{c}^{\bar{\sigma}}(0)\rho_{\mathrm{pf+re}}]}{s - \sigma i\Omega + \Gamma} \\ & + \lambda^2 \theta(-t) \mathcal{L}_t^{-1} \frac{\mathrm{Tr}[\tilde{c}^\sigma(0)\tilde{c}^{\bar{\sigma}}(0)\rho_{\mathrm{pf+re}}]}{s - \sigma i\Omega - \Gamma}, \end{aligned} \tag{B24}$$

where $\mathcal{L}_t^{-1}$ is the inverse Laplace transform which can be computed to obtain

$$C(t) = \lambda^2[(1-\sigma)/2 + \sigma n] \exp\{\sigma i\Omega t - \Gamma|t|\}, \tag{B25}$$

which, reintroducing the indices j used in the main text to label independent pseudoenvironments, leads to Eq. (14) by linearity.

3. Markovian regime

In this section, we review the limit in which the environment is Markovian. This regime is defined when all the memory effects described by the fermionic influence superoperator $\mathcal{F}(t, s, C^\sigma)$ in Eq. (6) are negligible. The Markovian limit can be recovered [17,68] in the quantum white-noise limit characterized by a constant spectral density and a constant equilibrium distribution, i.e.,

$$J(\omega) \mapsto \Gamma_0, \quad n_E^{\mathrm{eq}}(\omega) \mapsto n_0. \tag{B26}$$

In fact, these conditions, once inserted in Eq. (7), lead to

$$C^\sigma(t_2, t_1) = \Gamma_0[1 - \sigma + 2\sigma n_0]\delta(t_2 - t_1),$$

which, arguably, more commonly defines the Markov approximation. As shown in Ref. [68], in the case of a delta-correlated environment, the expression for the functional superoperator in Eq. (6) can be drastically simplified, leading to an effective generalized Lindblad equation of motion

$$\rho_S = -i[H_S, \rho_S] + \Gamma_0 \sum_{r=\pm} (1 - n_0) D_s^r[\rho_S^r] + n_0 D_{s^\dagger}^r[\rho_S^r], \tag{B27}$$

where $\rho_S^{r=\pm}$ are the projections of the density matrix into the space with even or odd fermionic parity. The dissipators $D_O^r[\cdot]$ are defined as

$$D_O^r[\cdot] = 2rO[\cdot]O^\dagger - O^\dagger O[\cdot] - [\cdot]O^\dagger O.$$

In non-Markovian regimes, the influence superoperator $\mathcal{F}$ is able to model more complex physical scenarios. For example, in the limit where the system is a single-level impurity, one recovers the single-impurity Anderson model, which is integrable in the noninteracting limit. Beyond this case, with, e.g., interacting or nonlinear impurities, one must resort to numerical methods.

This analysis can be easily adapted to the problem of tracing out the residual environments of the pseudofermion model defined in Eq. (B8). In fact, the residual environment of each pseudofermion is modeled as idealized white noise, and as a consequence, it can be traced out by simply considering the composite system+pseudofermions in place of S in Eq. (B27) leading to Eq. (16).

4. Correlations for a Lorentzian spectral density

We now consider the Lorentzian spectral density

$$J_L(\omega) = \frac{\Gamma W^2}{[(\omega - \omega_0)^2 + W^2]} = \frac{\Gamma W^2}{(\omega - a)(\omega - \bar{a})}, \tag{B28}$$

where $a = \omega_0 + iW$ and $\bar{a} = \omega_0 - iW$. With this spectral density, the correlation functions in Eq. (7) take the form

$$\begin{aligned} C^{\sigma=1}(t) &= \int_{-\infty}^{\infty} \frac{d\omega}{\pi} J_L(\omega) e^{i\omega t} n_{\beta\mu}(\omega), \\ C^{\sigma=-1}(t) &= \int_{-\infty}^{\infty} \frac{d\omega}{\pi} J_L(\omega) e^{-i\omega t} [1 - n_{\beta\mu}(\omega)] \end{aligned} \tag{B29}$$

and can be evaluated by noticing that the poles of the integrand are located at a, $\bar{a}$, and $\omega_k = \mu + ix_k$, where $x_k = (2k - 1)i\pi/\beta$, for $k \in \mathbb{N}$. For positive (negative) time arguments, we can close the contour in the upper (lower) complex plane to derive, for $t > 0$,

$$\begin{aligned} C^{\sigma=1}(t) = {} & 2i\Gamma W^2 \left[\frac{e^{iat}}{a - \bar{a}} \frac{1}{e^{\beta(a-\mu)} + 1} \right. \\ & \left. - \frac{1}{\beta} \sum_{k>0} \frac{e^{i\omega_k t}}{(\omega_k - a)(\omega_k - \bar{a})} \right], \\ C^{\sigma=1}(-t) = {} & 2i\Gamma W^2 \left[\frac{e^{-i\bar{a}t}}{a - \bar{a}} \frac{1}{e^{\beta(\bar{a}-\mu)} + 1} \right. \\ & \left. + \frac{1}{\beta} \sum_{k>0} \frac{e^{-2i\mu t} e^{i\omega_k t}}{(2\mu - \omega_k - a)(2\mu - \omega_k - \bar{a})} \right], \\ C^{\sigma=-1}(t) = {} & -2i\Gamma W^2 \left[\frac{e^{-i\bar{a}t}}{\bar{a} - a} \frac{e^{\beta(\bar{a}-\mu)}}{e^{\beta(\bar{a}-\mu)} + 1} \right. \\ & \left. + \frac{1}{\beta} \sum_{k>0} \frac{e^{-2i\mu t} e^{i\omega_k t}}{(2\mu - \omega_k - a)(2\mu - \omega_k - \bar{a})} \right], \\ C^{\sigma=-1}(-t) = {} & 2i\Gamma W^2 \left[\frac{e^{-\beta(\mu-a)} e^{iat}}{a - \bar{a}} \frac{1}{e^{\beta(a-\mu)} + 1} \right. \\ & \left. + \frac{1}{\beta} \sum_{k>0} \frac{e^{i\omega_k t}}{(\omega_k - a)(\omega_k - \bar{a})} \right]. \end{aligned} \tag{B30}$$

Noticing that $\bar{\omega}_k = 2\mu - \omega_k$, the above expressions are compatible with the general relation $C^\sigma(-t) = \bar{C}^\sigma(t)$.

$$C^{\sigma=-1}(-t) = 2i\Gamma W^2\left[\frac{e^{iat}}{a-\bar{a}}\left(1-\frac{1}{e^{\beta(a-\mu)}+1}\right) + \frac{1}{\beta}\sum_{k>0}\frac{e^{i\omega_k t}}{(\omega_k - a)(\omega_k - \bar{a})}\right] = 2i\Gamma W^2\frac{e^{iat}}{a-\bar{a}} - C^{\sigma=1}(t). \tag{B31}$$

Using the Matsubara expansion (see Ref. [1], Eq. (3.5), p. 110)

$$\frac{1}{e^{\beta x}+1} = \frac{1}{2} - \frac{1}{\beta}\sum_{k>0}\left(\frac{1}{x - ix_k} + \frac{1}{x + ix_k}\right), \tag{B32}$$

we can alternatively write, for $t > 0$,

$$\begin{aligned} C^{\sigma=1}(t) &= 2i\Gamma W^2\left\{\frac{e^{iat}}{a-\bar{a}}\left[\frac{1}{2} - \frac{1}{\beta}\sum_{k>0}\left(\frac{1}{a-\omega_k} + \frac{1}{a-2\mu+\omega_k}\right)\right] - \frac{1}{\beta}\sum_{k>0}\frac{e^{i\omega_k t}}{(\omega_k - a)(\omega_k - \bar{a})}\right\} \\ &= \left\{\frac{e^{iat}}{a-\bar{a}}\left[\frac{1}{2} - \frac{1}{\beta}\sum_{k>0}\left(\frac{1}{a-\omega_k} + \frac{1}{\omega_k - \bar{a}}\right)\right] - \frac{1}{\beta}\sum_{k>0}\frac{e^{i\omega_k t}}{(\omega_k - a)(\omega_k - \bar{a})}\right\} 2i\Gamma W^2 \\ &= 2i\Gamma W^2\left\{\frac{e^{iat}}{2(a-\bar{a})} - \frac{1}{\beta}\sum_{k>0}\frac{e^{i\omega_k t} - e^{iat}}{(\omega_k - a)(\omega_k - \bar{a})}\right\} \\ &= \frac{\Gamma W}{2}e^{i\mu t - Wt} + \frac{2i\Gamma W^2}{\beta}\sum_{k>0}\frac{e^{i\mu t - x_k t} - e^{i\mu t - Wt}}{(x_k - W)(x_k + W)}, \end{aligned} \tag{B33}$$

where we noticed that $1/(a - 2\mu + \omega_k) - 1/(\omega_k - \bar{a}) = 0$, $\forall k$. Using $C^\sigma(-t) = \bar{C}^\sigma(t)$, together with Eq. (B31), we can write, for $t > 0$,

$$\begin{aligned} C^{\sigma=-1}(t) &= \bar{C}^{\sigma=-1}(-t) \\ &= \Gamma W e^{-i\mu t - Wt} - \bar{C}^{\sigma=1}(t) \\ &= \frac{\Gamma W}{2}e^{-i\mu t - Wt} + \frac{2i\Gamma W^2}{\beta} \times \sum_{k>0}\frac{e^{-i\mu t - x_k t} - e^{-i\mu t - Wt}}{(x_k - W)(x_k + W)}. \end{aligned} \tag{B34}$$

Using $C^\sigma(-t) = \bar{C}^\sigma(t)$ again, we can extend these results to $t < 0$ to write, for any $t \in \mathbb{R}$,

$$C^\sigma_L(t) = C^\sigma_{\rm res} + \sum_{k>0} M^\sigma_k(t), \tag{B35}$$

where

$$\begin{aligned} C^\sigma_{\rm res} &= \frac{\Gamma W}{2}\exp\{\sigma i\mu t - W|t|\}, \\ M^\sigma_k(t) &= \frac{\mathrm{sgn}(t)2i\Gamma W^2}{\beta}\frac{e^{\sigma i\mu t - x_k|t|} - e^{\sigma i\mu t - W|t|}}{x_k^2 - W^2}, \end{aligned} \tag{B36}$$

where $\mathrm{sgn}(t) = t/|t|$, for $t \neq 0$, is the sign function. One interesting feature of this decomposition is that the pole at $x_k = W$ is explicitly removed from the notation (because of the presence of a corresponding zero in the numerator). The first line of Eq. (B36) reproduces the first line of Eq. (20) in the main text. In order to reproduce the second line of Eq. (20), there is a little more work to do. To achieve this, we use the identity in Eq. (B54) to write

$$\mathrm{sgn}(t)(e^{-x_k|t|} - e^{-W|t|}) = \frac{e^{\omega(t+|t|)} - e^{\omega(|t|-t)}}{e^{2\omega|t|} - 1}e^{-W|t|}(e^{-(x_k - W)|t|} - 1), \tag{B37}$$

for any $\omega \in \mathbb{C}$. For the specific choice $\omega = (W - x_k)/2$ we obtain

$$\mathrm{sgn}(t)(e^{-x|t|} - e^{-W|t|}) = e^{-(W+x)|t|/2}[e^{(W-x)t/2} - e^{-(W-x)t/2}], \tag{B38}$$

which, used in the second line of Eq. (B36), gives

$$M^\sigma_k(t) = \sum_{k>0}\frac{2i\Gamma W^2}{\beta}\frac{e^{-(W+x_k)|t|/2}}{(x_k^2 - W^2)} \times [e^{[i\sigma\mu + (W - x_k)/2]t} - e^{[i\sigma\mu - (W - x_k)/2]t}], \tag{B39}$$

which is the second line in Eq. (20).

We finish by noting that, in the zero-temperature limit ($\beta \to \infty$), the Matsubara frequencies x_k approach a continuum so that

$$M^\sigma(t) \overset{\beta\to\infty}{=} \mathrm{sgn}(t)\frac{i\Gamma W^2}{\pi}e^{i\sigma\mu t}\int_0^\infty dx\frac{e^{-x|t|} - e^{-W|t|}}{(x^2 - W^2)}. \tag{B40}$$

5. Correspondence to pseudoenvironments

Here we provide details about modeling the correlations $C^\sigma_{\rm res}(t)$ and $M^\sigma_k(t)$ in Eq. (20) using fermionic pseudoenvironments. We start from the resonant contribution $C^\sigma_{\rm res}(t)$. We want to find the parameters of a pseudoenvironment such that its free correlation function $C^\sigma_{\rm pf,res}(t)$, obtained using the identification $j \mapsto$ res in Eq. (14), fulfills

$$C^\sigma_{\rm res}(t) = C^\sigma_{\rm pf,res}(t). \tag{B41}$$

Using Eqs. (20) and (14), the equation above translates to

$$\frac{\Gamma W}{2}e^{i\sigma\mu t - W|t|} = \lambda^2_{\rm res}[(1-\sigma)/2 + \sigma n_{\rm res}]e^{i\sigma\Omega_{\rm res}t - \Gamma_{\rm res}|t|}. \tag{B42}$$

The equivalence in Eq. (B42) can be imposed by defining

$$\begin{aligned} n_{\rm res} &= 1/2, \\ \lambda_{\rm res} &= \sqrt{\Gamma W/(2n_{\rm res})}, \\ \Omega_{\rm res} &= \mu, \\ \Gamma_{\rm res} &= W, \end{aligned} \tag{B43}$$

which fully characterize the resonant pseudoenvironment. Similarly, for each k, the Matsubara contribution $M^\sigma_k(t)$ in Eq. (20) can be reproduced using two pseudoenvironments. Explicitly, identifying $j \to (k, r)$, $r = \pm$ in Eq. (14), we want

to impose

$$M_k^\sigma(t) = \sum_{r=\pm} C^\sigma_{\mathrm{pf},(k,r)}(t), \tag{B44}$$

which, using Eqs. (20) and (14), is equivalent to

$$\begin{aligned} &M_k e^{-(W+x_k)|t|/2} \sum_{r=\pm} r \exp\{[i\sigma\mu + r(W-x_k)/2]t\} \\ &= \sum_{r=\pm} \lambda^2_{k,r}[(1-\sigma)/2 + \sigma n_{k,r}] \exp\{i\sigma\Omega_{k,r}t - \Gamma_{k,r}|t|\}. \end{aligned} \tag{B45}$$

Imposing the equation above requires a bit of attention as the frequency $r(W-x_k)/2$ appearing in the expression of $M_k^\sigma(t)$ is *not* multiplied by the parameter σ as in the correlation for the pseudoenvironment. On the contrary, the coefficients multiplying the exponential in the correlation for the pseudoenvironment do depend on σ while M_k does not. Luckily, the Matsubara contributions $M_k^\sigma(t)$ are written in terms of a difference between exponentials with opposite frequencies which offers the opportunity to define the parameters characterizing the Matsubara pseudoenvironments as

$$\begin{aligned} n_{k,\pm} &= \Delta, \\ \lambda_{k,\pm} &= \sqrt{\pm M_k/\Delta}, \\ \Omega_{k,\pm} &= \mu \mp i(x_k - W)/2, \\ \Gamma_{k,\pm} &= (W + x_k)/2, \end{aligned} \tag{B46}$$

where $\Delta \in \mathbb{C}$ in the limit $|\Delta| \to \infty$ so that

$$\begin{aligned} C^\sigma_{\mathrm{pf},(k,r)}(t) = \frac{rM_k}{\Delta} e^{-(W+x_k)|t|/2}[(1-\sigma)/2 + \sigma\Delta] \\ \times \exp\{i\sigma[\mu - ir(x_k - W)/2]t\}, \end{aligned} \tag{B47}$$

which, inserted in Eq. (B44), leads to

$$\begin{aligned} M_k^\sigma(t) &= \frac{M_k}{\Delta} e^{-(W+x_k)|t|/2}[(1-\sigma)/2 + \sigma\Delta] \\ &\quad \times (e^{i\sigma[\mu - i(x_k-W)/2]t} - e^{i\sigma[\mu + i(x_k-W)/2]t}) \\ &= \frac{M_k}{\Delta} e^{-(W+x_k)|t|/2}[(1-\sigma)/2 + \sigma\Delta] \\ &\quad \times e^{i\sigma\mu t}(e^{\sigma[(x_k-W)/2]t} - e^{-\sigma[(x_k-W)/2]t}) \\ &= \frac{M_k}{\Delta} e^{-(W+x_k)|t|/2}[(1-\sigma)/2 + \sigma\Delta] \\ &\quad \times \sigma e^{i\sigma\mu t}(e^{[(x_k-W)/2]t} - e^{-[(x_k-W)/2]t}) \\ &\to M_k e^{-(W+x_k)|t|/2} \\ &\quad \times e^{i\sigma\mu t}(e^{[(x_k-W)/2]t} - e^{-[(x_k-W)/2]t}), \end{aligned} \tag{B48}$$

where, in the last step, the limit $|\Delta| \to \infty$ was taken. The above equation is equivalent to the expression for $M_k^\sigma(t)$ given in Eq. (20), thereby completing the proof. In numerical applications, the limit $\Delta \to \infty$ might introduce some numerical instabilities which can be regularized using intermediate values such that $\Delta \gg 1$.

Alternative formulation

Interestingly, it is also possible to build a pseudoenvironment which does not resort to any asymptotic parameter (Δ above). To achieve this, we need to introduce four pseudoenvironments to model each $M_k^\sigma(t)$ to impose

$$M_k^\sigma(t) = \sum_{r,\sigma'=\pm} C^\sigma_{\mathrm{pf},(k,r,\sigma')}(t), \tag{B49}$$

through the identification $j \to (k, r, \sigma')$, $r, \sigma' = \pm$, in Eq. (14). In order to fulfill Eq. (B49), we can choose the parameters

$$\begin{aligned} n_{k,r,\sigma'} &= (1+\sigma')/2, \\ \lambda_{k,r,\sigma'} &= \sqrt{rM_k}, \\ \Omega_{k,r,\sigma'} &= \mu - ir\sigma'(x_k - W)/2, \\ \Gamma_{k,r,\sigma'} &= (W + x_k)/2, \end{aligned} \tag{B50}$$

which correspond to a $\beta \to \sigma' \times \infty$ limit, so that [see Eq. (14)]

$$\begin{aligned} C^\sigma_{\mathrm{pf},(k,r,\sigma')}(t) = rM_k e^{-(W+x_k)|t|/2}\left[\frac{1-\sigma}{2} + \sigma\frac{1+\sigma'}{2}\right] \\ \times e^{i\sigma[\mu - ir\sigma'(x_k-W)/2]t}, \end{aligned} \tag{B51}$$

which, inserted in Eq. (B49), leads to

$$\begin{aligned} M_k^\sigma(t) &= \sum_{\sigma'} M_k e^{-(W+x_k)|t|/2}\left[\frac{1-\sigma}{2} + \sigma\frac{1+\sigma'}{2}\right] \\ &\quad \times (e^{i\sigma[\mu - i\sigma'(x_k-W)/2]t} - e^{i\sigma[\mu + i\sigma'(x_k-W)/2]t}) \\ &= \sum_{\sigma'} M_k e^{-(W+x_k)|t|/2}\delta_{\sigma\sigma'} \\ &\quad \times e^{i\sigma\mu t}(e^{\sigma\sigma'(x_k-W)t/2} - e^{-\sigma\sigma'(x_k-W)t/2}) \\ &= M_k e^{-(W+x_k)|t|/2} \\ &\quad \times e^{i\sigma\mu t}(e^{(x_k-W)t/2} - e^{-(x_k-W)t/2}), \end{aligned} \tag{B52}$$

which, similarly to the previous analysis, is equivalent to the expression for $M_k^\sigma(t)$ given in Eq. (20), thereby completing the proof.

6. Proof of an identity for the sign function

Let us define $\mathrm{sgn}(x) = x/|x|$ for $x \neq 0$. We have

$$\begin{aligned} e^{\omega(t+|t|)} - e^{\omega(|t|-t)} &\overset{t\geq 0}{=} e^{2\omega t} - 1 \\ &= e^{2\omega|t|} - 1 \\ &\overset{t\leq 0}{=} 1 - e^{-2\omega t} \\ &= 1 - e^{2\omega|t|}, \end{aligned} \tag{B53}$$

for any $\omega \in \mathbb{C}$. In a more compact notation, the previous equation can be written as

$$e^{\omega(t+|t|)} - e^{\omega(|t|-t)} = \mathrm{sgn}(t)(e^{2\omega|t|} - 1). \tag{B54}$$

APPENDIX C: EFFECTIVE MODEL FOR FAST DECAYING TERMS IN THE MATSUBARA CORRELATION

For bosonic environments, when a term in the Matsubara series has a decay rate which is larger than the highest frequency Ω_S which can be associated with the system, it is possible to approximate its effect on the system by adding an

extra dissipator to the master equation [28]. In this Appendix, we analyze the same limit in the case of a fermionic environment interacting with the system through the Lorentzian spectral density $J_L(\omega)$. In this case, the Matsubara series takes the form described in Eq. (20), i.e.,

$$M^{\sigma}(t) = \mathrm{sgn}(t)\frac{2i\Gamma W^2}{\beta}e^{i\sigma\mu t}\sum_{k>0}\frac{e^{-x_k|t|}-e^{-W|t|}}{\left(x_k^2-W^2\right)}, \tag{C1}$$

where $x_k = (2k-1)\pi/\beta$. As in the bosonic case, our starting point is the following limit representation of the Dirac delta [28]:

$$\delta(t) = \lim_{\epsilon\to 0}\frac{e^{-|t|/\epsilon}}{2\epsilon}. \tag{C2}$$

Among the exponentials present in the Matsubara series above, the ones which can be modeled with a delta contribution are those for which either $x_k \gg \Omega_S$ or $W \gg \Omega_S$. We note that the former possibility corresponds to a "high-temperature" limit [as it corresponds to $\beta\Omega_S \ll (2k-1)\pi$], while the latter corresponds to a "broad spectral density" limit. Whenever we are in one of these regimes, the corresponding contribution in the Matsubara series can be approximated as

$$M^{\sigma}_{\mathrm{eff}}(t) = \mathrm{sgn}(t)A_{\mathrm{eff}}\delta(t), \tag{C3}$$

where $A_{\mathrm{eff}} = i\Gamma_{\mathrm{eff}}$ in terms of an effective decay rate Γ_{eff}. We can now compute the corresponding contribution to the influence superoperator; that is, we can compute Eq. (6) with the replacement $C^{\sigma}(t_2,t_1) \mapsto M_{\mathrm{eff}}(t_2-t_1)$. We find

$$\mathcal{F}(t) = \int_0^t dt_2\int_0^{t_2} dt_1\ \mathcal{W}(t_2,t_1), \tag{C4}$$

where $\mathcal{W}(t_2,t_1) = \sum_{\sigma=\pm}\mathcal{A}^{\sigma}(t_2)\mathcal{B}^{\sigma}_{\mathrm{eff}}(t_2,t_1)$ with

$$\begin{aligned}\mathcal{A}^{\sigma}(t)[\cdot] &= \hat{s}^{\bar{\sigma}}(t)[\cdot] - \mathcal{P}_S[[\cdot]\hat{s}^{\bar{\sigma}}(t)],\\ \mathcal{B}^{\sigma}_{\mathrm{eff}}(t_2,t_1)[\cdot] &= -M^{\sigma}_{\mathrm{eff}}(t)\hat{s}^{\sigma}(t_1)\cdot - \bar{M}^{\bar{\sigma}}_{\mathrm{eff}}(t)\mathcal{P}_S[[\cdot]\hat{s}^{\sigma}(t_1)]\\ &= -A_{\mathrm{eff}}\delta(t)\hat{s}^{\sigma}(t_1)\cdot - \bar{A}_{\mathrm{eff}}\delta(t)\mathcal{P}_S[[\cdot]\hat{s}^{\sigma}(t_1)],\end{aligned}$$

where $t = t_2 - t_1 \geqslant 0$, which justifies the last step. We then obtain

$$\begin{aligned}W(t_2,t_1) = &-\delta(t)(s\cdot - \mathcal{P}_S[\cdot s])(A_{\mathrm{eff}}s^{\dagger}\cdot + \bar{A}_{\mathrm{eff}}\mathcal{P}_S[\cdot s^{\dagger}])/2\\ &-\delta(t)(s^{\dagger}\cdot - \mathcal{P}_S[\cdot s^{\dagger}])(A_{\mathrm{eff}}s\cdot + \bar{A}_{\mathrm{eff}}\mathcal{P}_S[\cdot s])/2.\end{aligned}$$

This means that, in the even or odd sector, in the Schrödinger picture, we have

$$\begin{aligned}\mathcal{F}(t) = &-tA_{\mathrm{eff}}(ss^{\dagger}\cdot - \cdot s^{\dagger}s \pm s\cdot s^{\dagger} \mp s^{\dagger}\cdot s)/2\\ &-tA_{\mathrm{eff}}(s^{\dagger}s\cdot - \cdot ss^{\dagger} \pm s^{\dagger}\cdot s \mp s\cdot s^{\dagger})/2\\ = &-A_{\mathrm{eff}}/2([ss^{\dagger}+s^{\dagger}s,\cdot])t,\end{aligned}$$

which, if s is such that it satisfies the fermionic anticommutation rules, is zero.

In conclusion, when a term in the Matsubara correlation function in Eq. (20) can be modeled as a delta function, it does not bring any effect on the system dynamics. For example, this implies that the Matsubara correlation function can be neglected when both the following conditions are satisfied: the high-temperature limit (i.e., $1/\beta$ much bigger than the highest frequency associated with the system) and a wide Lorentzian spectral density (i.e., with a width W much bigger than the highest frequency associated with the system).

FIG. 4. Schematics of the superfermion representation. Blue circles correspond to physical fermions, and orange circles correspond to auxiliary ones. They are combined in pairs to give one MPS site, shown as dashed ellipses. The pair on the left represents the system, while remaining sites represent the bath. Solid curves between sites indicate the long-ranged hopping terms induced by the Hamiltonian.

APPENDIX D: TENSOR NETWORK SIMULATION OF THE PSEUDOFERMION LINDBLAD MASTER EQUATION

Here we describe how to simulate the dynamics of the pseudofermion model [see Eq. (16)] using tensor networks. To do this, we are going to closely follow Ref. [12] and introduce a superfermion representation of the master equation and a SWAP-gate technique to treat long-ranged hopping which arises due to the use of an energy eigenbasis for the environments.

The superfermion representation is a way to map the fermionic master equation onto a non-Hermitian Schrödinger equation, similarly to purification techniques to simulate master equations [84]. In the superfermion representation, an extra auxiliary fermion is introduced for each physical fermion, thereby doubling the dimension of the Hilbert space. The arrangement of physical and auxiliary fermions is in principle

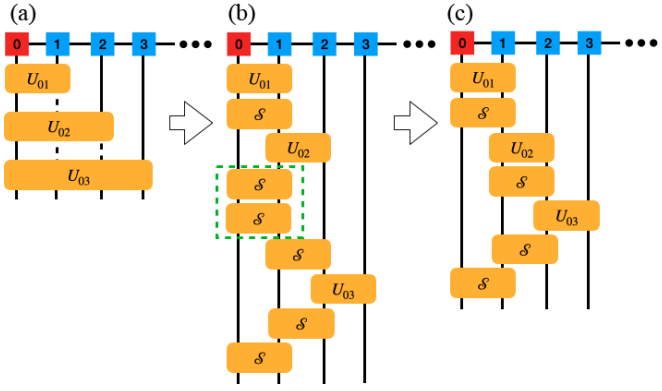

FIG. 5. Tensor network simulation of the pseudofermion master equation (16) using the superfermion representation and the SWAP-gate technique. (a) The density matrix of the composite system is represented as a MPS (red square for the system and blue squares for the pseudofermions). The Trotterized propagator acts on the MPS sequentially in the form of two-site gates which can be long ranged. (b) Each long-ranged gate can be decomposed into a series of two-site, nearest-neighbor gates which combine the SWAP gate $\mathcal{S}$ and the Trotterized propagator. Neighboring SWAP gates (in the dashed green box) can be combined to the identity operator, leading to the simplified version of the algorithm in (c).

arbitrary, but for the purpose of the tensor network simulation, it is beneficial to arrange them in an intertwined order; see Fig. 4.

A key object in this construction is the so-called left-vacuum state defined by

$$|I\rangle = |0\underline{0}, 0\underline{0}, \ldots, 0\underline{0}\rangle, \tag{D1}$$

where 0 (1) stands for an empty (filled) fermionic site and we have combined the physical fermion and the corresponding auxiliary one (marked by underlines) into pairs. One important formal tool needed to continue consists of the following conjugation rules:

$$d^\dagger|I\rangle = -\underline{d}|I\rangle, \quad d|I\rangle = \underline{d}^\dagger|I\rangle, \tag{D2}$$

where d and $\tilde{c}$ indicate system fermions and pseudofermions, respectively, while the auxiliary degrees of freedom are denoted by an additional underline ($\underline{d}$ and $\underline{\tilde{c}}$).

By applying the density matrix and master equation to $|I\rangle$ from the left and by using the conjugation rules above, one can write the following non-Hermitian Schrödinger equation:

$$d|\rho\rangle/dt = L|\rho\rangle, \tag{D3}$$

with $|\rho\rangle = \rho|I\rangle$ and

$$\begin{aligned} L = &-i\big(H^{(0)}_{S+\mathrm{pf}} - \underline{H}^{(0)}_{S+\mathrm{pf}}\big) \\ &+ \sum_j \Big\{ \Gamma_j n_j \Big[\tilde{c}^\dagger_j \underline{\tilde{c}}^\dagger_j - \frac{1}{2}(\tilde{c}_j \tilde{c}^\dagger_j + \underline{\tilde{c}}_j \underline{\tilde{c}}^\dagger_j) \Big] \\ &- \Gamma_j (1-n_j) \Big[\tilde{c}_j \underline{\tilde{c}}_j - \frac{1}{2}(\tilde{c}^\dagger_j \tilde{c}_j + \underline{\tilde{c}}^\dagger_j \underline{\tilde{c}}_j) \Big] \Big\}, \end{aligned}$$

where $H^{(0)}_{S+\mathrm{pf}}$ is given in Eq. (10) and $\underline{H}^{(0)}_{S+\mathrm{pf}}$ is obtained by replacing all operators in Eq. (10) by their underlined counterparts. The minus sign in front of $\underline{H}^{(0)}_{S+\mathrm{pf}}$ originates from the first commutator in the master equation in Eq. (16). Note that Eq. (D3) has no explicit dependence on the fermion parity, which is one of the main advantages of the superfermion representation.

To set a more efficient tensor network simulation, we combine a physical fermion and its partner into one single matrix product state (MPS) site, corresponding to a physical index of dimension four. The advantage of this representation is that all Lindblad terms in L are local, i.e., they act on a single MPS site.

On the contrary, the Hamiltonian characterizes hopping terms between the pseudofermions and the system in a so-called star geometry. To take this hopping into account, we use the SWAP gate

$$\mathcal{S} = (I_2 \otimes S \otimes I_2)(S \otimes S)(I_2 \otimes S \otimes I_2), \tag{D4}$$

which exchanges the local states of nearest-neighbor MPS sites. Here, I_2 is the 2×2 identity matrix, while the matrix S can be explicitly written as

$$S = \begin{pmatrix} 1 & 0 & 0 & 0 \\ 0 & 0 & 1 & 0 \\ 0 & 1 & 0 & 0 \\ 0 & 0 & 0 & -1 \end{pmatrix}, \tag{D5}$$

in the basis made by $\{|0\underline{0}\rangle, |0\underline{1}\rangle, |1\underline{0}\rangle, |1\underline{1}\rangle\}$. Intuitively, while S interchanges the states of two adjacent fermionic sites, the SWAP gate $\mathcal{S}$ swaps the states of two adjacent MPS sites (each consisting of two fermionic sites). For example, by labeling an MPS state as $|n_1\underline{n}_1, n_2\underline{n}_2\rangle$, the operator $I_2 \otimes S \otimes I_2$ swaps $\underline{n}_1 \leftrightarrow n_2$, the operator $S \otimes S$ swaps $n_1 \leftrightarrow n_2$ and $\underline{n}_1 \leftrightarrow \underline{n}_2$, and the operator $I_2 \otimes S \otimes I_2$ swaps $n_1 \leftrightarrow \underline{n}_2$, resulting in the expression presented in Eq. (D4).

With these definitions, any long-ranged two-site gate can be decomposed into a sequence of SWAP gates and nearest-neighbor gates, which can then be implemented with tensor networks efficiently. We have further used a second-order Trotter decomposition of the propagator and optimized the numerics by choosing the order of the gates to merge some of the SWAP gates arising due to long-range hopping into the identity operator. This algorithm is illustrated in Fig. 5.

The use of these MPS techniques results in the possibility of higher pseudofermion numbers, increasing the precision in modeling. For example, in the analysis of the Kondo regime presented in Fig. 3, we could fit the polynomial tail in the Matsubara contribution to the correlation function with good precision using three pseudofermions; see inset in Fig. 3(b). Using the MPS formalism described here, it was possible to compute the dynamics of the corresponding pseudofermion model, thereby improving the accuracy in the estimate of zero-frequency features such as those presented in Fig. 3(b) (dotted curve).

[1] M. D. Mahan, *Many-Particle Physics*, 3rd ed. (Kluwer Academic, New York, 2000).

[2] A. Zagoskin, *Quantum Theory of Many-Body Systems*, 2nd ed. (Springer International, Cham, Swizerland, 2014).

[3] S. N. Shevchenko, *Mesoscopic Physics Meets Quantum Engineering* (World Scientific, Singapore, 2019).

[4] P. Gehring, J. M. Thijssen, and H. S. J. van der Zant, Single-molecule quantum-transport phenomena in break junctions, Nat. Rev. Phys. **1**, 381 (2019).

[5] W. G. van der Wiel, S. De Franceschi, J. M. Elzerman, T. Fujisawa, S. Tarucha, and L. P. Kouwenhoven, Electron transport through double quantum dots, Rev. Mod. Phys. **75**, 1 (2002).

[6] M. W. Y. Tu and W.-M. Zhang, Non-Markovian decoherence theory for a double-dot charge qubit, Phys. Rev. B **78**, 235311 (2008).

[7] J. Jin, M. W. Y. Tu, W.-M. Zhang, and Y. Yan, Non-equilibrium quantum theory for nanodevices based on the Feynman–Vernon influence functional, New J. Phys. **12**, 083013 (2010).

[8] M. W.-Y. Tu, J.-H. Liu, and W.-M. Zhang, General analytical solution to exact fermion master equation, arXiv:1503.05376.

[9] H. T. Quan, Y.-x. Liu, C. P. Sun, and F. Nori, Quantum thermodynamic cycles and quantum heat engines, Phys. Rev. E **76**, 031105 (2007).

[10] M. Josefsson, A. Svilans, A. M. Burke, E. A. Hoffmann, S. Fahlvik, C. Thelander, M. Leijnse, and H. Linke,

A quantum-dot heat engine operating close to the thermodynamic efficiency limits, Nat. Nanotechnol. **13**, 920 (2018).
[11] N. Mosso, H. Sadeghi, A. Gemma, S. Sangtarash, U. Drechsler, C. Lambert, and B. Gotsmann, Thermal transport through single-molecule junctions, Nano Lett. **19**, 7614 (2019).
[12] M. Brenes, J. J. Mendoza-Arenas, A. Purkayastha, M. T. Mitchison, S. R. Clark, and J. Goold, Tensor-Network Method to Simulate Strongly Interacting Quantum Thermal Machines, Phys. Rev. X **10**, 031040 (2020).
[13] A. C. Hewson, *The Kondo Problem to Heavy Fermions* (Cambridge University Press, Cambridge, 1997).
[14] G. E. Topp, T. Brandes, and G. Schaller, Steady-state thermodynamics of non-interacting transport beyond weak coupling, Europhys. Lett. **110**, 67003 (2015).
[15] N. H. March and G. G. N. Angilella, *Exactly Solvable Models in Many-Body Theory* (World Scientific, Singapore, 2016).
[16] H.-P. Breuer and F. Petruccione, *The Theory of Open Quantum Systems* (Oxford University Press, Oxford, 2002).
[17] C. Gardiner and P. Zoller, *Quantum Noise: A Handbook of Markovian and Non-Markovian Quantum Stochastic Methods with Applications to Quantum Optics* (Springer Science, New York, 2004).
[18] W.-M. Zhang, P.-Y. Lo, H.-N. Xiong, M. W.-Y. Tu, and F. Nori, General Non-Markovian Dynamics of Open Quantum Systems, Phys. Rev. Lett. **109**, 170402 (2012).
[19] Y. Tanimura, Nonperturbative expansion method for a quantum system coupled to a harmonic-oscillator bath, Phys. Rev. A **41**, 6676 (1990).
[20] B. M. Garraway, Nonperturbative decay of an atomic system in a cavity, Phys. Rev. A **55**, 2290 (1997).
[21] J. Iles-Smith, N. Lambert, and A. Nazir, Environmental dynamics, correlations, and the emergence of noncanonical equilibrium states in open quantum systems, Phys. Rev. A **90**, 032114 (2014).
[22] H.-B. Chen, N. Lambert, Y.-C. Cheng, Y.-N. Chen, and F. Nori, Using non-Markovian measures to evaluate quantum master equations for photosynthesis, Sci. Rep. **5**, 12753 (2015).
[23] D. Tamascelli, A. Smirne, S. F. Huelga, and M. B. Plenio, Nonperturbative Treatment of non-Markovian Dynamics of Open Quantum Systems, Phys. Rev. Lett. **120**, 030402 (2018).
[24] A. Lemmer, C. Cormick, D. Tamascelli, T. Schaetz, S. F. Huelga, and M. B. Plenio, A trapped-ion simulator for spin-boson models with structured environments, New J. Phys. **20**, 073002 (2018).
[25] N. Lambert, S. Ahmed, M. Cirio, and F. Nori, Modelling the ultra-strongly coupled spin-boson model with unphysical modes, Nat. Commun. **10**, 3721 (2019).
[26] F. Mascherpa, A. Smirne, A. D. Somoza, P. Fernández-Acebal, S. Donadi, D. Tamascelli, S. F. Huelga, and M. B. Plenio, Optimized auxiliary oscillators for the simulation of general open quantum systems, Phys. Rev. A **101**, 052108 (2020).
[27] Y. Tanimura and R. Kubo, Time evolution of a quantum system in contact with a nearly Gaussian-Markoffian noise bath, J. Phys. Soc. Jpn. **58**, 101 (1989).
[28] A. Ishizaki and Y. Tanimura, Quantum dynamics of system strongly coupled to low-temperature colored noise bath: Reduced hierarchy equations approach, J. Phys. Soc. Jpn. **74**, 3131 (2005).
[29] A. Ishizaki and G. R. Fleming, Unified treatment of quantum coherent and incoherent hopping dynamics in electronic energy transfer: Reduced hierarchy equation approach, J. Chem. Phys. **130**, 234111 (2009).
[30] Y. Tanimura, Reduced hierarchical equations of motion in real and imaginary time: Correlated initial states and thermodynamic quantities, J. Chem. Phys. **141**, 044114 (2014).
[31] A. Fruchtman, N. Lambert, and E. Gauger, When do perturbative approaches accurately capture the dynamics of complex quantum systems? Sci. Rep. **6**, 28204 (2016).
[32] Y. Tanimura, Numerically "exact" approach to open quantum dynamics: The hierarchical equations of motion (HEOM), J. Chem. Phys. **153**, 020901 (2020).
[33] K. Nakamura and Y. Tanimura, Optical response of laser-driven charge-transfer complex described by Holstein–Hubbard model coupled to heat baths: Hierarchical equations of motion approach, J. Chem. Phys. **155**, 064106 (2021).
[34] J. Jin, X. Zheng, and Y. Yan, Exact dynamics of dissipative electronic systems and quantum transport: Hierarchical equations of motion approach, J. Chem. Phys. **128**, 234703 (2008).
[35] Z. Li, N. Tong, X. Zheng, D. Hou, J. Wei, J. Hu, and Y. Yan, Hierarchical Liouville-Space Approach for Accurate and Universal Characterization of Quantum Impurity Systems, Phys. Rev. Lett. **109**, 266403 (2012).
[36] C. Schinabeck, A. Erpenbeck, R. Härtle, and M. Thoss, Hierarchical quantum master equation approach to electronic-vibrational coupling in nonequilibrium transport through nanosystems, Phys. Rev. B **94**, 201407(R) (2016).
[37] C. Schinabeck, R. Härtle, and M. Thoss, Hierarchical quantum master equation approach to electronic-vibrational coupling in nonequilibrium transport through nanosystems: Reservoir formulation and application to vibrational instabilities, Phys. Rev. B **97**, 235429 (2018).
[38] N. Lambert, T. Raheja, S. Cross, P. Menczel, S. Ahmed, A. Pitchford, D. Burgarth, and F. Nori, QuTiP-BoFiN: A bosonic and fermionic numerical hierarchical-equations-of-motion library with applications in light-harvesting, quantum control, and single-molecule electronics, Phys. Rev. Res. **5**, 013181 (2023).
[39] J. K. Sowa, N. Lambert, T. Seideman, and E. M. Gauger, Beyond Marcus theory and the Landauer–Büttiker approach in molecular junctions. II. A self-consistent Born approach, J. Chem. Phys. **152**, 064103 (2020).
[40] Y. Tanimura, Stochastic Liouville, Langevin, Fokker–Planck, and master equation approaches to quantum dissipative systems, J. Phys. Soc. Jpn. **75**, 082001 (2006).
[41] L. Han, A. Ullah, Y.-A. Yan, X. Zheng, Y. Yan, and V. Chernyak, Stochastic equation of motion approach to fermionic dissipative dynamics. I. Formalism, J. Chem. Phys. **152**, 204105 (2020).
[42] A. Ullah, L. Han, Y.-A. Yan, X. Zheng, Y. Yan, and V. Chernyak, Stochastic equation of motion approach to fermionic dissipative dynamics. II. Numerical implementation, J. Chem. Phys. **152**, 204106 (2020).
[43] P. Strasberg, G. Schaller, T. L. Schmidt, and M. Esposito, Fermionic reaction coordinates and their application to an autonomous Maxwell demon in the strong-coupling regime, Phys. Rev. B **97**, 205405 (2018).
[44] E. Arrigoni, M. Knap, and W. von der Linden, Nonequilibrium Dynamical Mean-Field Theory: An Auxiliary Quantum Master Equation Approach, Phys. Rev. Lett. **110**, 086403 (2013).

[45] A. Dorda, M. Nuss, W. von der Linden, and E. Arrigoni, Auxiliary master equation approach to nonequilibrium correlated impurities, Phys. Rev. B **89**, 165105 (2014).

[46] I. Titvinidze, A. Dorda, W. von der Linden, and E. Arrigoni, Transport through a correlated interface: Auxiliary master equation approach, Phys. Rev. B **92**, 245125 (2015).

[47] A. Dorda, M. Ganahl, H. G. Evertz, W. von der Linden, and E. Arrigoni, Auxiliary master equation approach within matrix product states: Spectral properties of the nonequilibrium Anderson impurity model, Phys. Rev. B **92**, 125145 (2015).

[48] A. Dorda, M. Sorantin, W. von der Linden, and E. Arrigoni, Optimized auxiliary representation of non-Markovian impurity problems by a Lindblad equation, New J. Phys. **19**, 063005 (2017).

[49] D. M. Fugger, D. Bauernfeind, M. E. Sorantin, and E. Arrigoni, Nonequilibrium pseudogap Anderson impurity model: A master equation tensor network approach, Phys. Rev. B **101**, 165132 (2020).

[50] M. Cygorek, M. Cosacchi, A. Vagov, V. M. Axt, B. W. Lovett, J. Keeling, and E. M. Gauger, Simulation of open quantum systems by automated compression of arbitrary environments, Nat. Phys. **18**, 662 (2022).

[51] F. A. Pollock, C. Rodríguez-Rosario, T. Frauenheim, M. Paternostro, and K. Modi, Non-Markovian quantum processes: Complete framework and efficient characterization, Phys. Rev. A **97**, 012127 (2018).

[52] A. Strathearn, P. Kirton, D. Kilda, J. Keeling, and B. W. Lovett, Efficient non-Markovian quantum dynamics using time-evolving matrix product operators, Nat. Commun. **9**, 3322 (2018).

[53] D. Gribben, D. M. Rouse, J. Iles-Smith, A. Strathearn, H. Maguire, P. Kirton, A. Nazir, E. M. Gauger, and B. W. Lovett, Exact Dynamics of Nonadditive Environments in Non-Markovian Open Quantum Systems, PRX Quantum **3**, 010321 (2022).

[54] G. Pleasance, B. M. Garraway, and F. Petruccione, Generalized theory of pseudomodes for exact descriptions of non-Markovian quantum processes, Phys. Rev. Res. **2**, 043058 (2020).

[55] A. Garg, J. N. Onuchic, and V. Ambegaokar, Effect of friction on electron transfer in biomolecules, J. Chem. Phys. **83**, 4491 (1985).

[56] R. Martinazzo, B. Vacchini, K. H. Hughes, and I. Burghardt, Communication: Universal Markovian reduction of Brownian particle dynamics, J. Chem. Phys. **134**, 011101 (2011).

[57] M. P. Woods, R. Groux, A. W. Chin, S. F. Huelga, and M. B. Plenio, Mappings of open quantum systems onto chain representations and Markovian embeddings, J. Math. Phys. **55**, 032101 (2014).

[58] P. Strasberg, G. Schaller, N. Lambert, and T. Brandes, Nonequilibrium thermodynamics in the strong coupling and non-Markovian regime based on a reaction coordinate mapping, New J. Phys. **18**, 073007 (2016).

[59] M. Wertnik, A. Chin, F. Nori, and N. Lambert, Optimizing cooperative multi-environment dynamics in a dark-state-enhanced photosynthetic heat engine, J. Chem. Phys. **149**, 084112 (2018).

[60] A. W. Chin, A. Rivas, S. F. Huelga, and M. B. Plenio, Exact mapping between system-reservoir quantum models and semi-infinite discrete chains using orthogonal polynomials, J. Math. Phys. **51**, 092109 (2010).

[61] J. Prior, A. W. Chin, S. F. Huelga, and M. B. Plenio, Efficient Simulation of Strong System-Environment Interactions, Phys. Rev. Lett. **105**, 050404 (2010).

[62] D. Tamascelli, A. Smirne, J. Lim, S. F. Huelga, and M. B. Plenio, Efficient Simulation of Finite-Temperature Open Quantum Systems, Phys. Rev. Lett. **123**, 090402 (2019).

[63] A. Nüßeler, I. Dhand, S. F. Huelga, and M. B. Plenio, Efficient simulation of open quantum systems coupled to a Fermionic bath, Phys. Rev. B **101**, 155134 (2020).

[64] C. M. Bender and S. Boettcher, Real Spectra in Non-Hermitian Hamiltonians Having $\mathcal{PT}$ Symmetry, Phys. Rev. Lett. **80**, 5243 (1998).

[65] D. Trifonov, Pseudo-boson coherent and Fock states, in *Trends in Differential Geometry, Complex Analysis and Mathematical Physics*, edited by K. Sekigawa, V. S. Gerdjikov, and S. Dimiev (World Scientific, Singapore, 2009), pp. 241–250.

[66] F. Bagarello, Pseudo-bosons, Riesz bases and coherent states, J. Math. Phys. **51**, 023531 (2010).

[67] F. Bagarello, Linear pseudo-fermions, J. Phys. A: Math. Theor. **45**, 444002 (2012).

[68] M. Cirio, P.-C. Kuo, Y.-N. Chen, F. Nori, and N. Lambert, Canonical derivation of the fermionic influence superoperator, Phys. Rev. B **105**, 035121 (2022).

[69] W. Greiner and J. Reinhardt, *Field Quantization* (Springer-Verlag, Berlin, 1996).

[70] F. Schwarz, M. Goldstein, A. Dorda, E. Arrigoni, A. Weichselbaum, and J. von Delft, Lindblad-driven discretized leads for nonequilibrium steady-state transport in quantum impurity models: Recovering the continuum limit, Phys. Rev. B **94**, 155142 (2016).

[71] C. Schinabeck, Hierarchical quantum master equation approaches to nonequilibrium charge transport through single-molecule junctions, Ph.D. thesis, Friedrich-Alexander-Universität Erlangen-Nürnberg (FAU), 2019.

[72] J. R. Johansson, P. D. Nation, and F. Nori, QuTiP: An open-source Python framework for the dynamics of open quantum systems, Comput. Phys. Commun. **183**, 1760 (2012).

[73] J. R. Johansson, P. D. Nation, and F. Nori, QuTiP 2: A Python framework for the dynamics of open quantum systems, Comput. Phys. Commun. **184**, 1234 (2013).

[74] Y. Ashida, T. Shi, M. C. Bañuls, J. I. Cirac, and E. Demler, Solving Quantum Impurity Problems in and out of Equilibrium with the Variational Approach, Phys. Rev. Lett. **121**, 026805 (2018).

[75] Y. Ashida, T. Shi, M. C. Bañuls, J. I. Cirac, and E. Demler, Variational principle for quantum impurity systems in and out of equilibrium: Application to Kondo problems, Phys. Rev. B **98**, 024103 (2018).

[76] V. B. Ivan, S. Jeongmin, J. C. H. Chen, L. Arne, A. D. Wieck, T. Seigo, H.-S. Sim, and Y. Michihisa, Observation of the Kondo screening cloud, Nature (London) **579**, 210 (2020).

[77] C. P. Moca, I. Weymann, M. A. Werner, and G. Zarand, Kondo Cloud in a Superconductor, Phys. Rev. Lett. **127**, 186804 (2021).

[78] L. W. Smith, H. B. Chen, C. W. Chang, C. W. Wu, S. T. Lo, S. H. Chao, I. Farrer, H. E. Beere, J. P. Griffiths, G. A. C. Jones, D. A. Ritchie, Y. N. Chen, and T. M. Chen, Electrically Controllable Kondo Correlation in Spin-Orbit-Coupled Quantum Point Contacts, Phys. Rev. Lett. **128**, 027701 (2022).

[79] A. Damascelli, Z. Hussain, and Z.-X. Shen, Angle-resolved photoemission studies of the cuprate superconductors, Rev. Mod. Phys. **75**, 473 (2003).

[80] O. Y. Kolesnychenko, G. M. M. Heijnen, A. K. Zhuravlev, R. de Kort, M. I. Katsnelson, A. I. Lichtenstein, and H. van Kempen, Surface electronic structure of Cr(001): Experiment and theory, Phys. Rev. B **72**, 085456 (2005).

[81] A. D. Somoza, O. Marty, J. Lim, S. F. Huelga, and M. B. Plenio, Dissipation-Assisted Matrix Product Factorization, Phys. Rev. Lett. **123**, 100502 (2019).

[82] Q. Shi, Y. Xu, Y. Yan, and X. Meng, Efficient propagation of the hierarchical equations of motion using the matrix product state method, J. Chem. Phys. **148**, 174102 (2018).

[83] Y. Ke, R. Borrelli, and M. Thoss, Hierarchical equations of motion approach to hybrid fermionic and bosonic environments: Matrix product state formulation in twin space, J. Chem. Phys. **156**, 194102 (2022).

[84] U. Schollwöck, The density-matrix renormalization group in the age of matrix product states, Ann. Phys. (Amsterdam) **326**, 96 (2011).

[85] It has been written that the shortest and best way between two truths of the real domain often passes through the imaginary one [86].

[86] J. Hadamard, *An Essay on the Psychology of Invention in the Mathematical Field* (Princeton University Press, Princeton, NJ, 1945).